Applied Catalysis B: Environmental 98 (2010) 86–93

Contents lists available at ScienceDirect

Applied Catalysis B: Environmental

journal homepage: www.elsevier.com/locate/apcatb

Effect of preparation atmosphere of Pt–SnO_x/C catalysts on the catalytic activity for H_2/CO electro-oxidation

Guoxiong Wang*, Tatsuya Takeguchi*, Toshiro Yamanaka, Ernee Noryana Muhamad, Motofumi Mastuda, Wataru Ueda

Catalysis Research Center, Hokkaido University, Kita 21 Nishi 10, Kita-ku, Sapporo 001-0021, Japan

ARTICLE INFO

Article history:
Received 9 February 2010
Received in revised form 19 April 2010
Accepted 13 May 2010
Available online 20 May 2010

Keywords:
Pt–SnO_x/C catalyst
Preparation atmosphere
CO tolerance

ABSTRACT

Pt–SnO_x/C catalysts were prepared in a polyol process under Ar, sequential Ar and air, and air atmospheres in combination with a high temperature reduction treatment. The composition, structure, morphology and oxidation state of the prepared catalysts were characterized by Inductively Coupled Plasma-Atom Emission Spectroscopy, X-ray diffraction, scanning transmission electron microscopy and X-ray photoelectron spectroscopy. The electrochemical activities were evaluated by CO stripping voltammetry and single cell test in combination with *in situ* IR reflection absorption spectroscopy (IRRAS). The polyol-synthesized Pt–SnO_x/C catalysts prepared under different atmospheres had a similar bulk composition, particle size and lattice parameter, however, the Pt–SnO_x/C catalyst prepared under Ar atmosphere possessed a greater proportion of Sn(II) species than the other Pt–SnO_x/C catalysts. Electrochemical and *in situ* IRRAS measurements indicated that the Pt–SnO_x/C catalyst under Ar atmosphere had the greatest CO tolerance in proton electrolyte fuel cell among the Pt–SnO_x/C catalysts.

1. Introduction

Pt-based binary catalysts are usually used as anode catalysts in polymer electrolyte fuel cell (PEFC) for electro-oxidation of H_2/CO mixture [1]. Pt–Ru catalyst has exhibited excellent CO tolerance because Ru is more active than Pt for providing OH_{ads} at low potentials and thus promotes electro-oxidation of CO_{ads} on Pt site [2]. However, due to the competition of OH_{ads} production on Ru with CO_{ads} formation, the overpotential on Pt–Ru catalyst greatly increases with CO concentration of the H_2/CO mixture [3]. Since CO does not interfere with OH_{ads} formation on SnO_x site [3], Pt–SnO_x catalyst is considered as one of the promising candidates and has been widely investigated [3–15].

In order to obtain a great electro-catalytic activity, a high dispersion with a high metal loading is usually required for carbon-supported Pt-based catalysts [16]. Various preparation methods have been developed to achieve this objective [17–23]. In recent years, the polyol method using ethylene glycol (EG) as both solvent and reductant of metallic precursors has been widely investigated [20,21,24–28]. The preparation atmosphere of Pt–Ru/C catalyst obtained in the polyol process was reported to have a remarkable effect on the catalytic activity for methanol electro-oxidation, and the inert atmosphere could produce a greater proportion of metallic Pt and Ru than the oxidation atmosphere, which was critical for a superior catalytic activity [24]. It is well known that there are different oxidation states of tin, i.e., Sn(IV), Sn(II) and Sn(0), in Pt–SnO_x catalyst, and the oxidation state of tin in Pt–SnO_x catalyst has been reported to play a critical role in reforming and dehydrogenation reactions [29]. For H_2/CO electro-oxidation, both the alloyed Sn and the non-alloyed SnO_x (including Sn(II) and Sn(IV)) adjacent to Pt in Pt–SnO_x/C catalyst exhibited a promotional effect via the bi-functional mechanism [10]. It was also reported that there was strong chemical interaction between Pt and SnO_x on the electro-oxidation of H_2/CO mixture, and the catalytic activity was dependent on the pre-treatment atmosphere [13]. In view of the mild reduction ability of EG [21,30], it is interesting to investigate the effect of preparation atmosphere of Pt–SnO_x/C catalysts obtained in the polyol process on catalytic activity for H_2/CO electro-oxidation.

In this work, Pt–SnO_x/C catalysts were prepared in a polyol process under Ar, sequential Ar and air, and air atmospheres in combination with a high temperature reduction treatment. The prepared catalysts were characterized by Inductively Coupled Plasma-Atom Emission Spectroscopy (ICP-AES), X-ray diffraction (XRD), scanning transmission electron microscopy (STEM) and X-ray photoelectron spectroscopy (XPS). CO stripping voltammetry in combination with *in situ* infrared reflection absorption spectroscopy (IRRAS) was conducted to evaluate CO_{ads} electro-oxidation activity on the Pt–SnO_x/C catalysts as well as the

* Corresponding authors. Tel.: +81 11 706 9165; fax: +81 11 706 9163.
E-mail addresses: wanggx@cat.hokudai.ac.jp (G. Wang), takeguch@cat.hokudai.ac.jp (T. Takeguchi).

0926-3373/$ – see front matter © 2010 Elsevier B.V. All rights reserved.
doi:10.1016/j.apcatb.2010.05.016

electrochemical surface area of the catalysts. Pure H_2 or H_2/CO mixture with different CO concentrations was fed into the anode of a single cell to measure the PEFC performance and CO overpotential of the Pt–SnO_x/C catalysts.

2. Experimental

2.1. Catalyst preparation

Four Pt–SnO_x/C catalysts were prepared in a polyol process [31] under Ar, sequential Ar and air, and air atmospheres in combination with a high temperature reduction treatment, respectively. The typical preparation procedure under Ar atmosphere was as follows: a calculated amount of $H_2PtCl_6{\cdot}6H_2O$, $SnCl_2{\cdot}2H_2O$ and Vulcan XC-72 carbon black was dissolved into EG in a three-necked flask. Then the pH value of the solution was increased to about 13 with 1 M NaOH solution, followed by stirring and purging with high-purity (99.99%) Ar. The solution was heated to 165 °C at a rate of 10 K min^{-1} and kept at that temperature for 4 h, and then the solution was cooled to 90 °C. HCl solution was then added to adjust the pH value to about 2 and the solution was kept at 90 °C for 24 h. Finally, the obtained catalyst was filtered, washed, and dried. The catalyst was denoted as Pt–SnO_x/C–Ar catalyst. The second Pt–SnO_x/C catalyst was prepared in the same procedure except that the precursor solution was kept at 165 °C under Ar atmosphere for 2 h and then air atmosphere for 2 h, and the catalyst was denoted as Pt–SnO_x/C–Ar + air catalyst. The third Pt–SnO_x/C catalyst was prepared in the same process as that described above under air atmosphere and denoted as Pt–SnO_x/C–air catalyst. For comparison, the Pt–SnO_x/C–Ar catalyst was treated in 5% H_2/Ar at 250 °C for 2 h, and the obtained catalyst was denoted as Pt–SnO_x/C–H_2 catalyst. The nominal Pt loading was 40 wt% and the nominal atomic ratio of Sn and Pt was 1:3 in the above Pt–SnO_x/C catalysts. 40 wt% Pt/C catalyst was also prepared in the polyol process and denoted as Pt/C catalyst.

2.2. Physicochemical characterization

The actual loadings of Pt and Sn in the Pt/C and Pt–SnO_x/C catalysts were determined by ICP-AES (Shimadzu ICPE-9000). XRD patterns of the catalysts were recorded with a Powder X-ray diffractometer (RIGAKU, RINT 2000) using Cu Kα radiation with a Ni filter. The tube current was 40 mA with a tube voltage of 40 kV. The angle was extended from 10° to 85° and was varied using a step size of 0.01°, accumulating data for 6 s per step. Catalyst morphology was investigated by using a STEM (Hitachi HD-2000) at 200 kV and 30 μA. XPS measurements were carried out using a JEOL JPS-9010MC spectrometer with a Mg Kα radiation source. The Pt (4f) and Sn (3d) signals were collected. The position of the C (1s) peak, that is, 284.2 eV for the JEOL JPS-9010MC spectrometer, was used to correct the binding energies of the Pt and Pt–SnO_x/C catalysts.

2.3. CO stripping voltammetry and in situ IRRAS measurements

CO stripping voltammetry measurement was carried out in a 250 mL three-electrode cell (HR200, Hokuto Denko Corp.) at 25 °C. A commercial glassy carbon (GC) electrode (HR2-D1-GC-5, 5 mm in diameter, 0.196 cm^2, Hokuto Denko Corp.), a Pt-wire electrode (Hokuto Denko Corp.), and a saturated calomel electrode (SCE, Hokuto Denko Corp.) were used as a working electrode, a counter electrode and a reference electrode, respectively. The potential of the working electrode was controlled by an Iviumstat Electrochemical Interface System (Ivium Technologies B.V.). Five mg of the Pt/C or Pt–SnO_x/C catalyst was dispersed in a mixture of 2 mL water, 2 mL ethanol and 50 μL Nafion solution (5 wt%, Aldrich) with ultrasonic stirring to form a homogeneous ink [32]. The catalyst layer was prepared by dropping 20 μL of the ink onto a GC disk electrode by a microsyringe and drying at room temperature. All potential values in this paper are referred to a reversible hydrogen electrode (RHE). After the electrolyte (0.5 M $HClO_4$) had been supplied with CO for 20 min, bulk CO in the electrolyte was removed by bubbling high-purity Ar through it for another 30 min. CO stripping voltammetry was performed between 0.018 and 1.2 V with a scan rate of 10 mV s^{-1}. The calculated peak charge Q_{CO} was used to compare the electrochemical surface area of the catalysts, which was obtained with the assumption of a monolayer of linearly adsorbed CO and charge density required for electro-oxidation of 0.42 mC cm^{-2} [33].

The *in situ* IRRAS measurements were carried out in a home-made PTFE cell with a CaF_2 optical window using a JASCO FT/IR-6100 spectrometer equipped with a TGS detector [27,34]. A gold disk (10 mm in diameter) was used as an electrode substrate for IRRAS measurements. The catalyst layers were deposited on the gold electrode surface with the same method as described for the CO stripping voltammetry experiments. Adsorption of CO was conducted firstly by bubbling CO into the cell for 20 min under potential control at 0.0 V, then high-purity Ar was bubbled for 35 min to remove the CO dissolved in the electrolyte solution. Then the electrode was pushed onto the CaF_2 prism window with the thin-layer geometry to reduce the IR absorption by aqueous solution. The *in situ* IR spectra were recorded with a scan rate of 0.25 mV s^{-1}, and 25 interferograms were co-added to each spectrum. To obtain CO_{ads} spectra, the spectrum recorded at the potential where CO_{ads} is completely oxidized was used a reference spectrum. To follow the production of CO_2, the spectrum recorded at 0.0 V was used as a reference spectrum.

2.4. Membrane and electrode assembly (MEA) fabrication

A P50T carbon paper (Ballard Material Products Inc.) was employed as the anode and cathode backing layer [28]. Carbon black ink containing Vulcan XC-72 carbon black and polytetrafluoroethylene (PTFE, Aldrich) was painted onto the backing layer to form a microporous layer. The carbon black loading was about 1.2 mg cm^{-2} and the PTFE content in the microporous layer was 40 wt%. To fabricate the anode catalyst layer, the Pt–SnO_x/C (or Pt/C) catalyst and Nafion solution was ultrasonically suspended in water and then brushed onto the microporous layer at 70 °C. The resulting loading of the Pt–SnO_x/C catalyst was 1.2 ± 0.1 mg cm^{-2} and the Nafion content was 10 wt%. Then a Nafion solution was brushed onto the surface of the anode catalyst layer with a dry ionomer loading of about 0.5 mg cm^{-2}. In all cases, an identical cathode catalyst layer was prepared by the same procedure as that described above. The resulting 40 wt% Pt/C (Johnson Matthey Corp.) loading was 1.0 ± 0.1 mg cm^{-2} and the Nafion content was the same as in the anode catalyst layer. Finally, the anode and cathode (2.2 cm × 2.2 cm) were placed onto the two sides of a Nafion NRE-212 membrane (Aldrich) and hot-pressed at 135 °C and 4 MPa for 10 min to form the MEA.

2.5. Single cell test

The MEA with two silicon sheets was assembled into a single cell with graphite flow field plates and copper end plates attached with a heater (FC05-01SP, ElectroChem, Inc.) [28]. The single cell was installed on a Fuel Cell Testing Equipment (Kofloc Corp.), which was equipped with mass flow-rate controllers and humidifiers for the reactant gases. The polarization curves were recorded by a KFM 2030 impedance meter (Kikusui Corp.). Pure H_2 (or H_2/CO mixture) and oxygen at a flow-rate of 80 mL min^{-1} were fed into the anode and cathode at ambient pressure. During the measurement, the sin-

Table 1
Data obtained from ICP-AES and XRD analyses.

Catalyst	Pt (wt%)	Sn (wt%)	Sn/Pt atomic ratio	Pt (2 2 0) peak (°)	Lattice parameter (Å)	Mean crystallite size (nm)
Pt/C	41.6	–	–	67.62 ± 0.02	3.915 ± 0.001	2.6
Pt–SnO_x/C–air	36.7	8.5	0.38	67.32 ± 0.03	3.931 ± 0.002	2.5
Pt–SnO_x/C–Ar + air	37.1	8.1	0.36	67.33 ± 0.01	3.930 ± 0.001	2.4
Pt–SnO_x/C–Ar	36.3	7.8	0.35	67.23 ± 0.02	3.935 ± 0.001	2.3
Pt–SnO_x/C–H_2	38.6	8.5	0.36	66.15 ± 0.02	3.992 ± 0.001	5.7

gle cell was operated at 75 °C, and the anode and cathode humidifier temperatures were set at 75 and 70 °C, respectively.

3. Results and discussion

The actual Pt and Sn loadings and Sn/Pt bulk atomic ratio in the Pt/C and Pt–SnO_x/C catalysts are listed in Table 1. The Pt/C catalyst had a Pt loading of 41.6%, while all the Pt–SnO_x/C catalysts had a similar Pt loading and Sn/Pt bulk atomic ratio, which allows us to investigate the effect of the preparation atmosphere of Pt–SnO_x/C catalysts on the catalytic activity for H_2/CO electro-oxidation. Fig. 1 shows XRD patterns of the Pt/C and Pt–SnO_x/C catalysts. Compared with the Pt/C catalyst, the Pt–SnO_x/C–air, Pt–SnO_x/C–Ar + air and Pt–SnO_x/C–Ar catalysts displayed two small diffraction peaks of SnO_2 (1 0 1) and SnO_2 (2 1 1) at around 34° and 52°, respectively, while the intensity of the two diffraction peaks of the Pt–SnO_x/C–Ar catalyst was lower than that of the Pt–SnO_x/C–air and Pt–SnO_x/C–Ar + air catalysts. For the Pt–SnO_x/C–H_2 catalyst, the two diffraction peaks of SnO_2 (1 0 1) and SnO_2 (2 1 1) were not observed. Furthermore, weak superlattice reflections ascribed to the Pt_3Sn phase were observed in the diffractograms of the Pt–SnO_x/C–H_2 catalyst, those corresponding to the (2 1 0) and (2 1 1) peaks of the Pt_3Sn phase [15] being depicted in the inset to Fig. 1, while these superlattice reflections were not observed in the diffractograms of the Pt–SnO_x/C–air, Pt–SnO_x/C–Ar + air and Pt–SnO_x/C–Ar catalysts, which is possibly ascribed to that these reflections were so weak in these Pt–SnO_x/C catalysts that they may not be observable above the background from scattering from the carbon support and/or SnO_2 [9]. All the Pt–SnO_x/C catalysts displayed a negative shift in Pt diffraction peaks, which possibly originates from Pt–Sn alloy formation [35]; however, the peak shifts were different, indicative of different lattice parameters of the Pt–SnO_x/C catalysts. The Pt (2 2 0) peak position was obtained in the XRD pattern and used for calculation of lattice parameter (a) as follows:

$$a = \frac{\sqrt{2}\lambda_{K\alpha}}{\sin\theta_{max}} \quad (1)$$

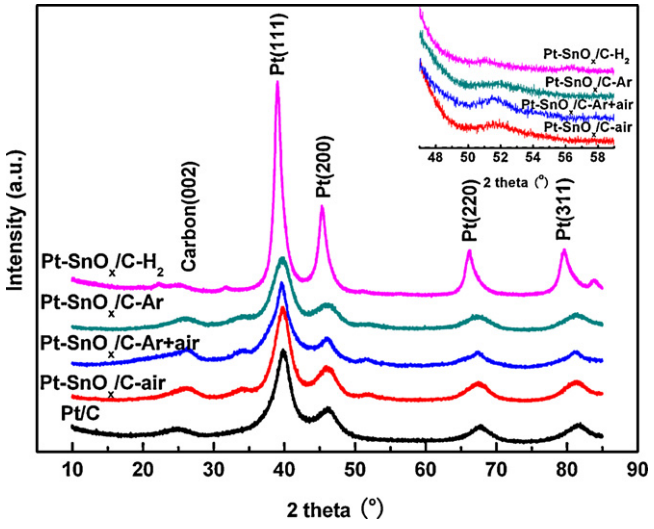

Fig. 1. XRD patterns of Pt/C and Pt–SnO_x/C catalysts.

Table 1 lists the lattice parameter and mean crystallite size obtained from XRD patterns. The lattice parameter of the Pt–SnO_x/C–air, Pt–SnO_x/C–Ar + air and Pt–SnO_x/C–Ar catalysts were 3.931 ± 0.002, 3.930 ± 0.001 and 3.935 ± 0.001 Å, respectively, which suggested that the catalyst preparation atmosphere in the polyol process had negligible effect on the Pt–Sn alloy formation. For the Pt–SnO_x/C–H_2 catalyst, the lattice parameter was greatly increased and reached 3.992 ± 0.001 Å, suggesting that the subsequent high temperature reduction treatment by H_2 greatly improved the Pt–Sn alloy formation. The Pt/C and Pt–SnO_x/C catalysts also showed some difference in mean crystallite size. The mean crystallite size of the Pt/C and Pt–SnO_x/C–air catalysts was calculated to be 2.6 and 2.5 nm, while the mean crystallite size of the Pt–SnO_x/C–Ar + air and Pt–SnO_x/C–Ar catalysts was slightly decreased to 2.4 and 2.3 nm. Compared with that of the Pt–SnO_x/C–Ar catalyst, the mean crystallite size of the Pt–SnO_x/C–H_2 catalyst was greatly increased to 5.7 nm, indicative of obvious agglomeration after the high temperature reduction treatment. Fig. 2 shows STEM images of the Pt/C and Pt–SnO_x/C catalysts. It can be observed that the Pt/C, Pt–SnO_x/C–air, Pt–SnO_x/C–Ar + air and Pt–SnO_x/C–Ar catalysts had similar morphology with uniform distribution on the carbon support, while the Pt–SnO_x/C–H_2 catalyst had an obvious agglomeration.

XPS was carried out to investigate the oxidation state of Pt and Sn and surface composition in the Pt–SnO_x/C catalysts. Fig. 3 shows the Pt 4f and Sn 3d spectra of the Pt/C and Pt–SnO_x/C catalysts. The Pt $4f_{7/2}$ XPS line is fitted with a convolution of three peaks corresponding to three different oxidation states of Pt. The results obtained by deconvoluting the XPS spectra are summarized in Table 2. The first peak (71.1 eV) is assigned to the reduced Pt(0) species, whereas the second peak (72.0 eV) is associated with oxidized Pt atoms from PtO species. The third peak (73.6 eV) is assigned to PtO_2 species [36]. As listed in Table 2, the Pt–SnO_x/C–air, Pt–SnO_x/C–Ar + air and Pt–SnO_x/C–Ar catalysts had a greater portion of Pt(0) species than the Pt/C catalyst, suggesting that the oxidation state of platinum was modified by the presence of Sn species [37]. It should be noted that the metallic Pt proportion in the Pt–SnO_x/C–air, Pt–SnO_x/C–Ar + air and Pt–SnO_x/C–Ar catalysts was similar, which was different from the XPS results of the Pt–Ru/C catalysts prepared under different atmospheres [24]. Compared with the Pt–SnO_x/C–Ar catalyst, the metallic Pt proportion in the Pt–SnO_x/C–H_2 catalyst was further improved by the subsequent high temperature reduction treatment.

The Sn 3d spectra of different Pt–SnO_x/C catalysts are shown in Fig. 3(b). The peak binding energy of the Sn $3d_{5/2}$ in the Pt–SnO_x/C–air, Pt–SnO_x/C–Ar + air, Pt–SnO_x/C–Ar and Pt–SnO_x/C–H_2 was 486.6, 486.7, 486.8 and 486.0 eV, respectively. Sn(0) species can appear at a binding energy value as high as 486.0 eV [13], so the Pt–SnO_x/C–H_2 catalyst had a great portion of metallic Sn species. Compared with that of the Pt–SnO_x/C–air catalyst, the binding energy of the Pt–SnO_x/C–Ar catalyst had a positive shift of 0.2 eV, indicative of a greater proportion of Sn(II) species

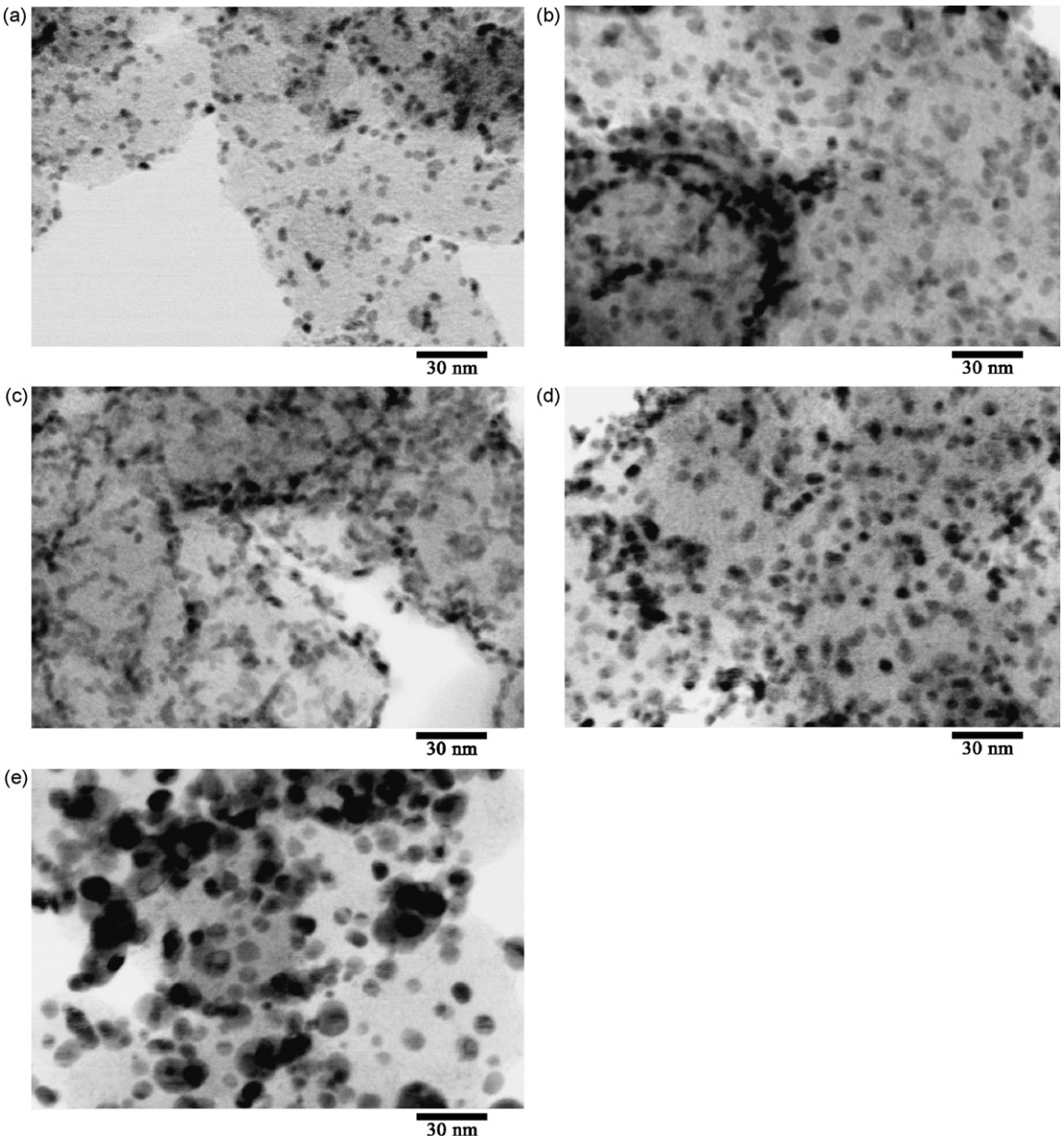

Fig. 2. STEM images of Pt/C (a), Pt–SnO_x/C–air (b), Pt–SnO_x/C–Ar + air (c), Pt–SnO_x/C–Ar (d) and Pt–SnO_x/C–H_2 (e) catalysts.

Table 2
XPS analysis results of Pt 4f spectra in the Pt/C and Pt–SnO_x/C catalysts.

Catalyst	Binding energy (eV)	Peak half width (eV)	Assignment	Atomic ratio (%)	Sn/Pt atomic ratio
Pt/C	71.1	1.5	Pt	27.0	–
	72.0	1.9	PtO	27.2	
	73.6	3.5	PtO_2	45.8	
Pt–SnO_x/C–air	71.1	1.5	Pt	46.3	0.71
	72.0	2.1	PtO	30.1	
	73.9	3.7	PtO_2	23.6	
Pt–SnO_x/C–Ar + air	71.1	1.5	Pt	44.8	0.55
	72.1	2.1	PtO	32.2	
	73.9	3.6	PtO_2	23.0	
Pt–SnO_x/C–Ar	71.1	1.5	Pt	47.6	0.64
	72.1	2.0	PtO	29.3	
	73.8	3.6	PtO_2	23.1	
Pt–SnO_x/C–H_2	71.1	1.5	Pt	62.9	0.62
	72.2	2.1	PtO	17.3	
	73.6	3.6	PtO_2	19.8	

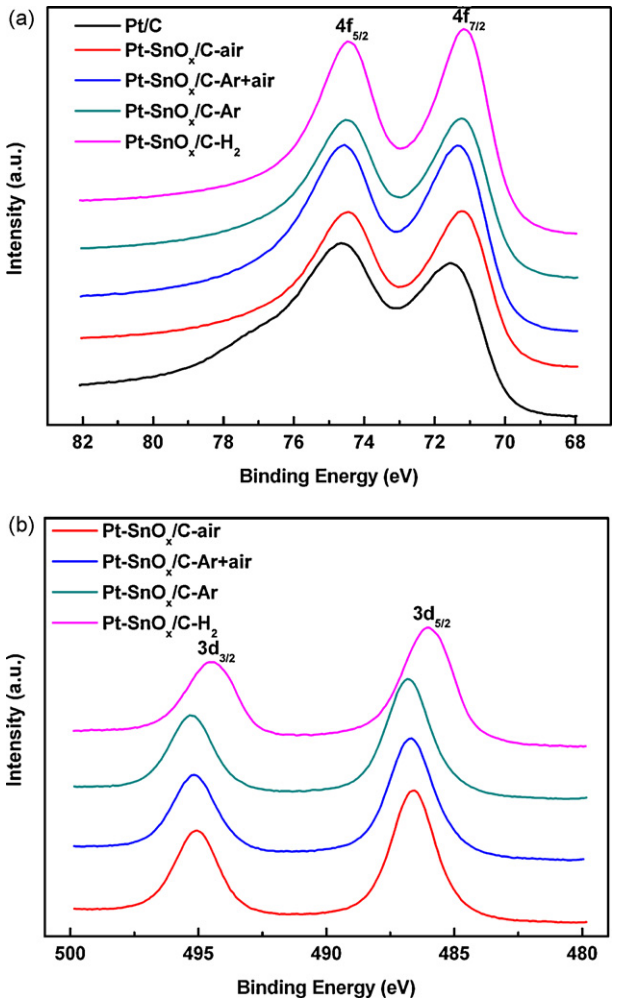

Fig. 3. Pt 4f (a) and Sn 3d (b) signals in the XPS spectra of Pt/C and Pt–SnO_x/C catalysts.

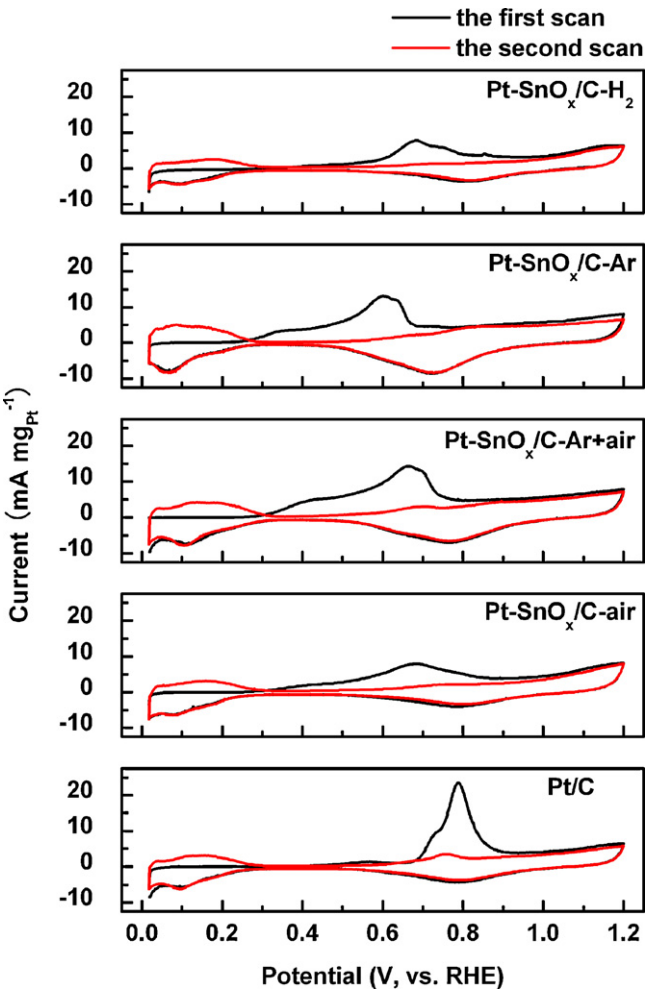

Fig. 4. CO stripping voltammetry of Pt/C and Pt–SnO_x/C catalysts in 0.5 M $HClO_4$ at 25 °C. Scan rate: 10 mV s^{-1}.

[38]. For the Pt–SnO_x/C–Ar + air catalyst, the subsequent exposure to air also caused a negative shift of 0.1 eV on binding energy compared with that of the Pt–SnO_x/C–Ar catalyst, suggesting that a part of Sn(II) species was oxidized to Sn(IV) species. During Pt–SnO_x/C catalyst preparation in the polyol process, $SnCl_2$ was protected by EG molecules and Cl^- was replaced by EG molecules [39]. A part of Sn^{2+} was reduced to Sn(0) by EG and formed Pt–Sn alloy, while the other part of Sn^{2+} was hydrolyzed to $Sn(OH)_2$, $Sn(OH)_2$ was prone to be further oxidized to $Sn(OH)_4$ by oxygen in air, so the Pt–SnO_x/C–Ar catalyst possessed a much greater portion of Sn(II) species than the Pt–SnO_x/C–air catalyst.

The surface composition of the Pt–SnO_x/C catalysts was estimated from the XPS by using peak areas normalized on the basis of sensitivity factors, and the results are also listed in Table 2. Although the Sn/Pt bulk atomic ratio determined by ICP-AES in the Pt–SnO_x/C catalysts was similar, the Sn/Pt surface atomic ratio estimated by XPS was significantly changed with the catalyst preparation atmosphere in the polyol process. Compared with that in the Pt–SnO_x/C–Ar catalyst, the subsequent high temperature reduction treatment caused a slightly lower Sn/Pt surface atomic ratio in the Pt–SnO_x/C–H_2 catalyst. In addition, for all the Pt–SnO_x/C catalysts, the Sn/Pt surface atomic ratio was apparently greater than the Sn/Pt bulk atomic ratio, indicative of significant surface Sn enrichment, which may be due to that the Sn element has a lower surface free energy than Pt element [40]. This result also agrees with the reported results [40,41].

Fig. 4 shows CO stripping voltammetries on the Pt/C and Pt–SnO_x/C catalysts in 0.5 M $HClO_4$ at 25 °C. There were a weak peak at 0.566 V (preoxidation peak) and a strong peak at 0.789 V (main peak) on the Pt/C catalyst, and the preoxidation peak could be ascribed to preferential oxidation of bridge adsorbed CO (CO_B), preferential oxidation of linearly adsorbed CO (CO_L) at or near defect sites, etc [42]. Compared with the Pt/C catalysts, all of the Pt–SnO_x/C catalysts showed negative shifts on the onset and peak potentials of CO_{ads} electro-oxidation, indicating that the catalytic activity of the Pt–SnO_x/C catalysts for CO_{ads} electro-oxidation was superior to that of the Pt/C catalyst. The Pt–SnO_x/C–Ar + air and Pt–SnO_x/C–Ar catalysts had a quite similar CO stripping voltammetry shape, while the peak potential of CO_{ads} electro-oxidation on the Pt–SnO_x/C–Ar + air and Pt–SnO_x/C–Ar catalysts was 0.666 and 0.601 V, respectively. Considering that the subsequent exposure to air caused the conversion of Sn(II) to Sn(IV), the difference on the peak potential between the Pt–SnO_x/C–Ar + air and Pt–SnO_x/C–Ar catalysts indicated that the chemical interaction between Pt and Sn(II) species played a critical role in the catalytic activity for CO_{ads} electro-oxidation. The electrochemical surface areas (ESAs) of the Pt/C, Pt–SnO_x/C–air, Pt–SnO_x/C–Ar + air, Pt–SnO_x/C–Ar and Pt–SnO_x/C–H_2 catalysts were calculated to be 43.2, 26.3, 49.4, 41.5 and 20.6 m^2 g^{-1} Pt, respectively. Although the Pt–SnO_x/C–air, Pt–SnO_x/C–Ar + air and Pt–SnO_x/C–Ar catalysts have similar particle size, the Pt–SnO_x/C–air catalyst had a much lower ESA than the Pt–SnO_x/C–Ar + air and Pt–SnO_x/C–Ar catalysts, indicating that a greater fraction of Pt surface was covered by Sn species [43].

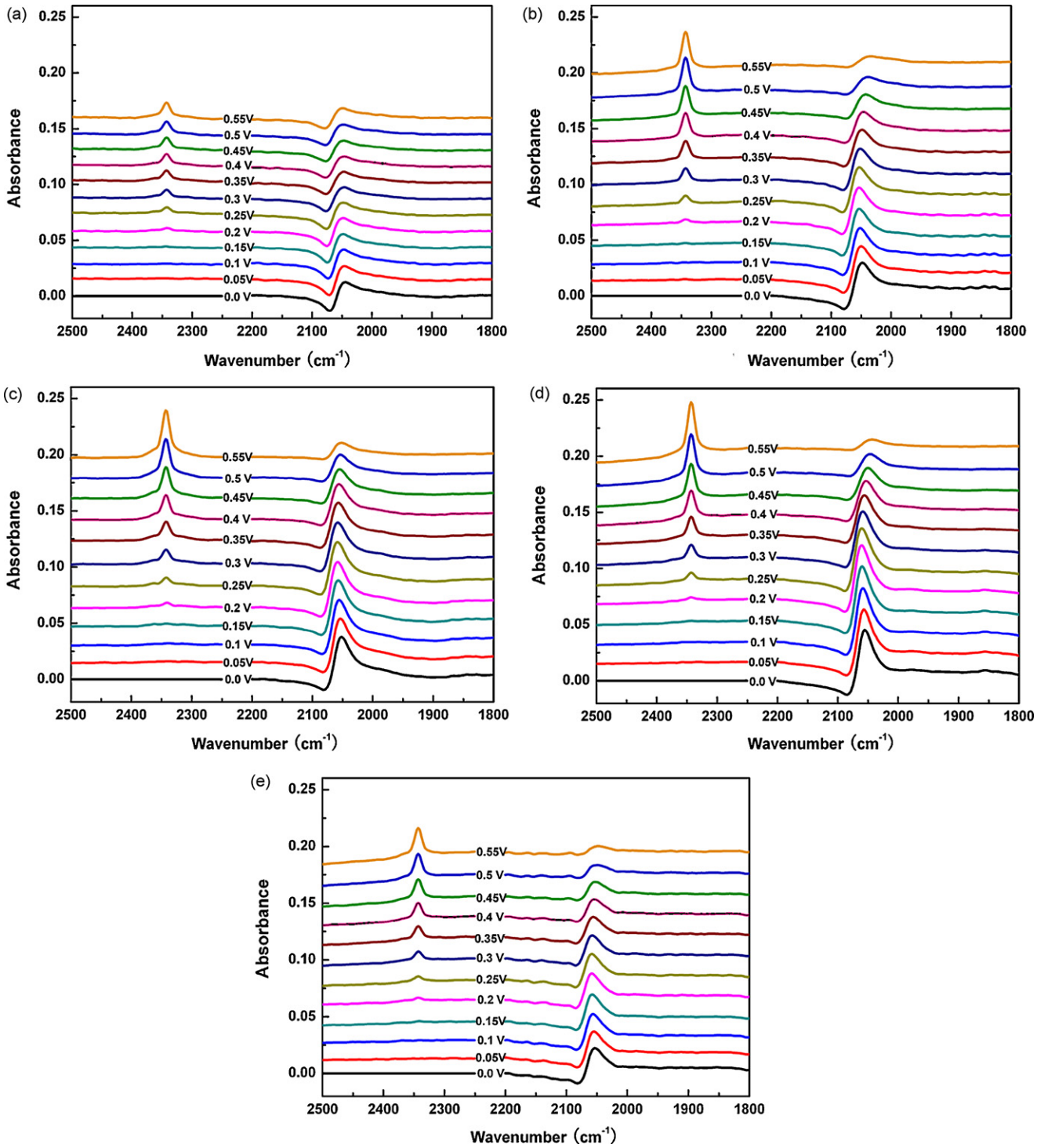

Fig. 5. *In situ* IRRAS spectra of Pt/C (a), Pt–SnO_x/C–air (b), Pt–SnO_x/C–Ar + air (c), Pt–SnO_x/C–Ar (d) and Pt–SnO_x/C–H_2 (e) catalysts deposited on a gold substrate surface. Potentials are indicated in the middle of each spectrum.

Because the Pt–SnO_x/C–H_2 catalyst had the largest particle size with an obvious agglomeration, the ESA of the Pt–SnO_x/C–H_2 catalyst was the smallest among the Pt/C and Pt–SnO_x/C catalysts.

A series of respective FTIR spectra for the Pt and Pt–SnO_x/C catalysts is shown in Fig. 5. For the Pt/C catalyst, the band at around 2044 cm^{-1} was assigned to CO_L on the Pt sites [10]. At 0.20 V, a new peak appeared at around 2343 cm^{-1}, which can be assigned to C–O stretching mode of CO_2, the product of CO_{ads} electrooxidation. In the case of the Pt–SnO_x/C catalysts (Fig. 5(b)–(e)), the spectral features were similar to that of the Pt/C catalyst. More details about the promotional effect of Sn species are provided by the potential dependence of the C–O stretching frequency, as shown in Fig. 6. At low potentials, the C–O stretching frequency on all the Pt–SnO_x/C catalysts was higher than that on the Pt/C catalyst, and the appearance of the higher frequency mode of CO on the Pt–SnO_x/C catalysts indicated a weakly adsorbed state of CO on Pt sites, which was probably caused by chemical interaction between Pt and Sn atoms (ligand effect) or the repulsive CO_{ads}–OH_{ads} interaction [4]. Although the Pt–SnO_x/C–air, Pt–SnO_x/C–Ar + air and Pt–SnO_x/C–Ar catalysts had a similar lattice

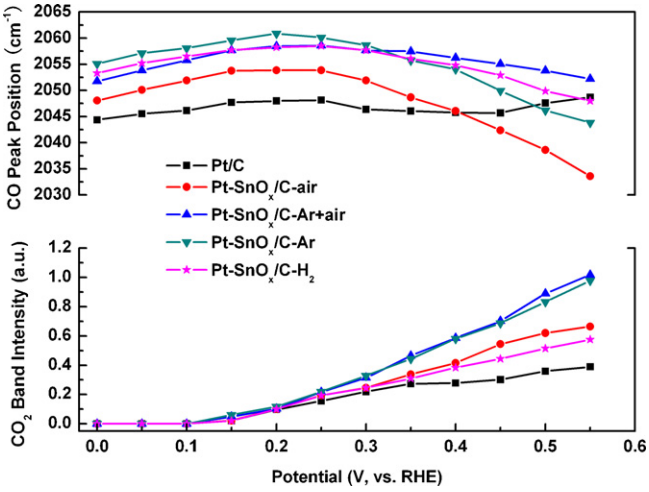

Fig. 6. The CO band peak position and integrated IR intensities for CO_2 generated as a function of electrode potential on Pt/C and Pt–SnO_x/C catalysts.

parameter, the C–O stretching frequency on these catalysts was much different, suggesting that the shift on the C–O stretching frequency in the Pt–SnO_x/C catalysts was ascribed to the repulsive CO_{ads}–OH_{ads} interaction. The Pt–SnO_x/C–Ar catalyst had the highest C–O stretching frequency, indicating that Sn(II) species were more beneficial to weaken the adsorption of CO on Pt sites than Sn(IV) and Sn(0) species. The linear shift of the C–O stretching frequency with the applied potential below 0.25 V, the Stark effect, was observed on the Pt/C and Pt–SnO_x/C catalysts. Above 0.25 V, the C–O stretching frequency on the Pt–SnO_x/C catalysts shifted down because the CO_{ads} coverage on these catalysts began to decrease sharply with increasing potential, while the C–O stretching frequency on the Pt/C catalyst decreased slightly and then increased quickly from 0.45 V, which was due to that CO_{ads} electro-oxidation on the Pt/C catalyst had a pre-ignition region at low potentials and a main region at high potentials [10]. Fig. 6 also shows integrated IR intensities for CO_2 generated as function of electrode potential on the Pt/C and Pt–SnO_x/C catalysts. Interestingly, CO electro-oxidation started at the same potential on the Pt/C and different Pt–SnO_x/C catalysts, which was caused by the integrating nature of the measurement of CO_2 in solution in the thin-layer geometry of the IR cell and the unsteady, fundamentally time-dependent nature of CO_{ads} electro-oxidation on pure Pt surfaces [10]. The increase in the CO_2 band intensity on the Pt/C catalyst with potential was much smaller than that on the Pt–SnO_x/C catalysts, which is similar to the reported results [10]. At low potentials ($0.15\,V \le E \le 0.30\,V$), the Pt–$SnO_x$/C–Ar catalyst had the greatest CO_2 intensity among the Pt–SnO_x/C catalysts due to the lowest onset potential of CO_{ads} electro-oxidation as shown in Fig. 4. At high potentials ($0.35\,V \le E \le 0.55\,V$), the CO_2 intensity on the Pt–SnO_x/C–Ar + air catalyst was slightly greater than that on the Pt–SnO_x/C–Ar catalyst, which was ascribed to a greater ESA of the Pt–SnO_x/C–Ar + air catalyst.

Single cell performance was carried out to investigate the electrochemical activities of the Pt/C and Pt–SnO_x/C catalysts toward H_2/CO mixtures with different CO concentrations, as shown in Figs. 7 and 8. Fig. 7(a) and (b) shows PEFC performance of the Pt/C and Pt–SnO_x/C catalysts under H_2 and 100 ppm CO-contaminated H_2, respectively. When the anode was fed with pure H_2, the Pt/C, Pt–SnO_x/C–Ar + air and Pt–SnO_x/C–Ar catalysts showed a similar performance, while the Pt–SnO_x/C–air and Pt–SnO_x/C–H_2 catalysts gave a poor performance compared with the Pt/C catalyst, which was ascribed to the low ESAs of the catalysts. When the anode was fed with 100 ppm CO-contaminated H_2, the Pt/C cat-

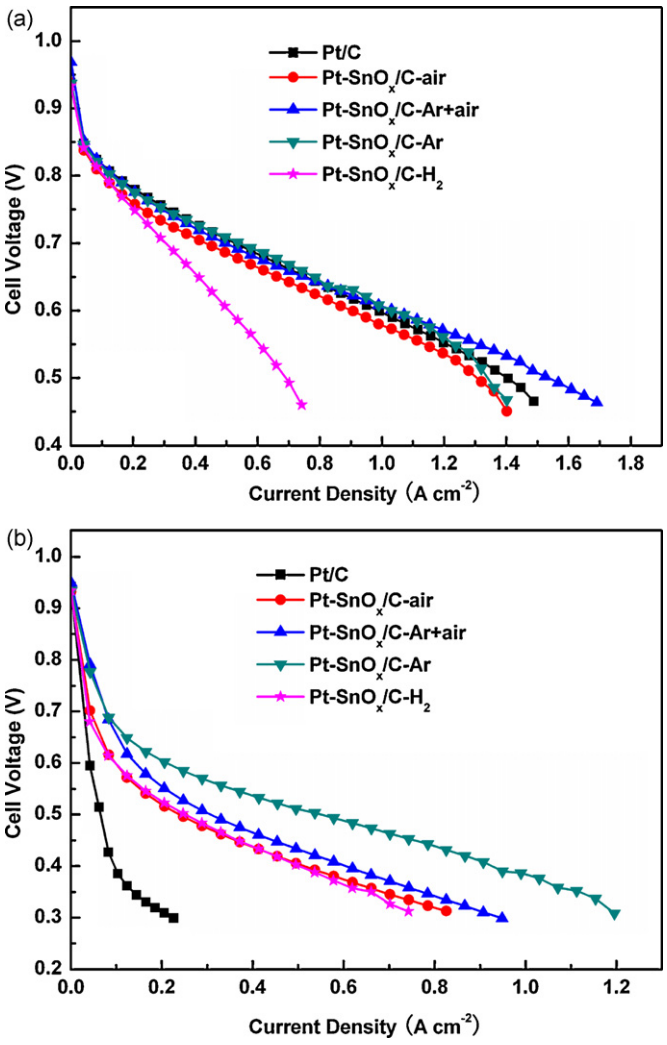

Fig. 7. Curves of cell voltage vs. current density of PEFC fed with H_2 (a) and 100 ppm CO-contaminated H_2 (b).

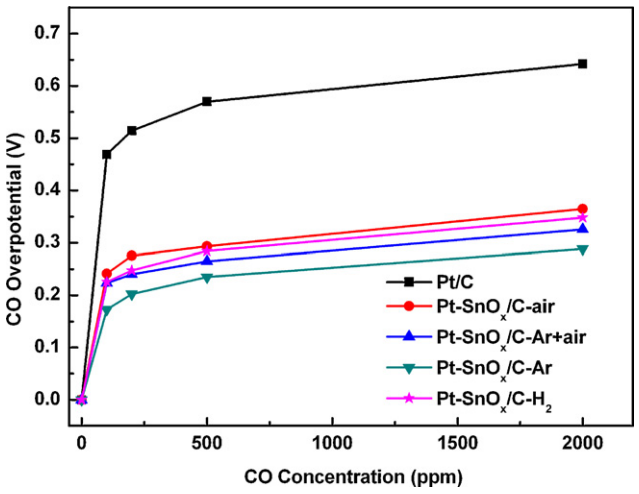

Fig. 8. The CO overpotential of Pt/C and Pt–SnO_x/C catalysts at $0.2\,A\,cm^{-2}$ under different CO concentrations.

alyst showed a great performance decline, while all the Pt–SnO_x/C catalysts gave an improved CO tolerance compared with the Pt/C catalyst, indicating the promotional role of Sn species in the Pt–SnO_x/C catalysts. At a current density of 0.2 A cm^{-2}, the cell voltage of the Pt/C, Pt–SnO_x/C–air, Pt–SnO_x/C–Ar + air, Pt–SnO_x/C–Ar and Pt–SnO_x/C–H_2 catalysts were 0.313, 0.519, 0.554, 0.604 and 0.525 V, respectively. The Pt–SnO_x/C–Ar catalyst showed the most pronounced promotional role for H_2/CO electro-oxidation among the four Pt–SnO_x/C catalysts, in agreement with the CO stripping voltammetry results.

Calculation of CO overpotential in the anode, which is a conventional method for comparing CO tolerance of different anode catalysts [28], is obtained by the following equation:

$$\eta_{CO} = E_{H_2} - E_{H_2/CO} \quad (2)$$

where E_{H_2} and $E_{H_2/CO}$ are the cell voltages under pure H_2 and CO-contaminated H_2, respectively. Fig. 8 shows the CO overpotential of the Pt/C and Pt–SnO_x/C catalysts at 0.2 A cm^{-2} with CO concentrations ranging from 100 to 2000 ppm. When the CO concentration in the H_2/CO mixture is increased, the rate of the CO electro-oxidation depends on the rate of OH_{ads} formation neighboring to Pt. Because both the alloyed Sn and the non-alloyed SnO_x in Pt–SnO_x/C catalyst were more effective to produce OH_{ads} than Pt at low potentials, all the Pt–SnO_x/C catalysts showed a much lower CO overpotential than the Pt/C catalyst at different CO concentrations. Although the Pt–SnO_x/C–Ar + air catalyst had a greater ESA than the Pt–SnO_x/C–Ar catalyst, the CO overpotential of the Pt–SnO_x/C–Ar catalyst was lower than that of the Pt–SnO_x/C–Ar + air catalyst due to the chemical interaction between Pt and Sn(II) species.

4. Conclusions

Pt–SnO_x/C catalysts with different dominant oxidation states of tin were prepared under different atmospheres in the polyol process in combination with a high temperature reduction treatment. ICP-AES analysis results showed that all the Pt–SnO_x/C catalysts had a similar Pt loading and Sn/Pt bulk atomic ratio. XRD and STEM results indicated that the preparation atmosphere in the polyol process had a negligible effect on the lattice parameter and particle size of the Pt–SnO_x/C catalyst, and that the subsequent reduction treatment in 5% H_2/Ar at 250 °C greatly improved the Pt–Sn alloy formation and, at the same time, caused obvious agglomeration. XPS results suggested that the preparation atmosphere did not alter the oxidation state distribution of Pt, but resulted in a great proportion of Sn(II) species in the Pt–SnO_x/C–Ar catalyst. On the basis of CO stripping voltammetry and *in situ* IRRAS results, the most negative shift in peak potential, the highest C–O stretching frequency and the greatest CO_2 band intensity at low potentials ($0.15\,V \le E \le 0.30\,V$) on the Pt–$SnO_x$/C–Ar catalyst indicated that the chemical interaction between Pt and Sn(II) species played a critical role in the catalytic activity for CO_{ads} electro-oxidation. Single cell test showed that the Pt–SnO_x/C–Ar catalyst exhibited the greatest CO tolerance among the Pt/C and different Pt–SnO_x/C catalysts.

Acknowledgments

This study was supported by Strategic Development of PEFC Technologies for Practical Application Grant Program in 08002063-0 from the NEDO of Japan. We thank Ms. Nozomi Takeda at the OPEN FACILITY of Hakkaido Unversity Sousei Hall for the ICP-AES measurement.

References

[1] T.R. Ralph, M.P. Hogarth, Platinum Met. Rev. 46 (2002) 117–135.
[2] M. Watanabe, S. Motoo, J. Electroanal. Chem. 60 (1975) 275–283.
[3] H.A. Gasteiger, N.M. Markovic, P.N. Ross, J. Phys. Chem. 99 (1995) 8945–8949.
[4] V.R. Stamenkovic, M. Arenz, C.A. Lucas, M.E. Gallagher, P.N. Ross, N.M. Markovic, J. Am. Chem. Soc. 125 (2003) 2736–2745.
[5] B.E. Hayden, M.E. Rendall, O. South, J. Am. Chem. Soc. 125 (2003) 7738–7742.
[6] E.M. Crabb, R. Marshall, D. Thompsett, J. Electrochem. Soc. 147 (2000) 4440–4447.
[7] A.C. Boucher, N. Alonso-Vante, F. Dassenoy, W. Vogel, Langmuir 19 (2003) 10885–10891.
[8] S. Tillmann, G. Samjeske, K.A. Friedrich, H. Baltruschat, Electrochim. Acta 49 (2003) 73–83.
[9] V. Radmilovic, T.J. Richardson, S.J. Chen, P.N. Ross Jr., J. Catal. 232 (2005) 199–209.
[10] M. Arenz, V. Stamenkovic, B.B. Blizanac, K.J. Mayrhofer, N.M. Markovic, P.N. Ross, J. Catal. 232 (2005) 402–410.
[11] T. Matsui, T. Okanishi, K. Fujiwara, K. Tsutsui, R. Kikuchi, T. Takeguchi, K. Eguchi, Sci. Technol. Adv. Mater. 7 (2006) 524–530.
[12] T. Matsui, K. Fujiwara, T. Okanishi, R. Kikuchi, T. Takeguchi, K. Eguchi, J. Power Sources 155 (2006) 152–156.
[13] T. Okanishi, T. Matsui, T. Takeguchi, R. Kikuchi, K. Eguchi, Appl. Catal. A: Gen. 298 (2006) 181–187.
[14] D.-H. Lim, D.-H. Choi, W.-D. Lee, H.-I. Lee, Appl. Catal. B: Environ. 89 (2009) 484–493.
[15] S. García-Rodríguez, F. Somodi, I. Borbáth, J.L. Margitfalvi, M.A. Peña, J.L.G. Fierro, S. Rojas, Appl. Catal. B: Environ. 91 (2009) 83–91.
[16] T.R. Ralph, M.P. Hogarth, Platinum Met. Rev. 46 (2002) 3–14.
[17] H. Bönnemann, W. Brijoux, R. Brinkmann, E. Dinjus, T. Jouβen, B. Korall, Angew. Chem. Int. Ed. 30 (1991) 1312–1314.
[18] K. Lasch, L. Jörissen, J. Garche, J. Power Sources 84 (1999) 225–230.
[19] A.J. Dickinson, L.P.L. Carrette, J.A. Collins, K.A. Friedrich, U. Stimming, Electrochim. Acta 47 (2002) 3733–3739.
[20] Z.H. Zhou, S.L. Wang, W.J. Zhou, G.X. Wang, L.H. Jiang, W.Z. Li, S.Q. Song, J.G. Liu, G.Q. Sun, Q. Xin, Chem. Commun. 3 (2003) 394–395.
[21] C. Bock, C. Paquet, M. Couillard, G.A. Botton, B.R. MacDougall, J. Am. Chem. Soc. 126 (2004) 8028–8037.
[22] B.H. Wu, D. Hu, Y.J. Kuang, B. Liu, X.H. Zhang, J.H. Chen, Angew. Chem. Int. Ed. 48 (2009) 4751–4754.
[23] B.Z. Fang, N.K. Chaudhari, M.-S. Kim, J.H. Kim, J.-S. Yu, J. Am. Chem. Soc. 131 (2009) 15330–15338.
[24] H.Q. Li, G.Q. Sun, Y. Gao, Q. Jiang, Z.Q. Jia, Q. Xin, J. Phys. Chem. C 111 (2007) 15192–15200.
[25] G.X. Wang, G.Q. Sun, Z.H. Zhou, J.G. Liu, Q. Wang, S.L. Wang, J.S. Guo, S.H. Yang, Q. Xin, B.L. Yi, Electrochem. Solid State Lett. 8 (2005) A12–A16.
[26] Q. Wang, G.Q. Sun, L. Cao, L.H. Jiang, G.X. Wang, S.L. Wang, S.H. Yang, Q. Xin, J. Power Sources 177 (2008) 142–147.
[27] G.X. Wang, T. Takeguchi, Y. Zhang, E.N. Muhamad, M. Sadakane, S. Ye, W. Ueda, J. Electrochem. Soc. 156 (2009) B862–B869.
[28] G.X. Wang, T. Takeguchi, E.N. Muhamad, T. Yamanaka, M. Sadakane, W. Ueda, J. Electrochem. Soc. 156 (2009) B1348–B1353.
[29] N. Nava, P. Del Angel, J. Salmones, E. Baggio-Saitovitch, P. Santiago, Appl. Surf. Sci. 253 (2007) 9215–9220.
[30] D. Larcher, R. Patrice, J. Solid State Chem. 154 (2000) 405–411.
[31] L.H. Jiang, Z.H. Zhou, W.Z. Li, W.J. Zhou, S.Q. Song, H.Q. Li, G.Q. Sun, Q. Xin, Energy Fuel 18 (2004) 866–871.
[32] Q. Wang, G.Q. Sun, L.H. Jiang, Q. Xin, S.G. Sun, Y.X. Jiang, S.P. Chen, Z. Jusys, R.J. Behm, Phys. Chem. Chem. Phys. 9 (2007) 2686–2696.
[33] Y. Takasu, T. Fujiwara, Y. Murakami, K. Sasaki, M. Oguri, T. Asaki, W. Sugimoto, J. Electrochem. Soc. 147 (2000) 4421–4427.
[34] S. Ye, T. Haba, Y. Sato, K. Shimazu, K. Uosaki, Phys. Chem. Chem. Phys. 1 (1999) 3653–3659.
[35] E. Antolini, F. Colmati, E.R. Gonzalez, Electrochem. Commun. 9 (2007) 398–404.
[36] D.L. Wang, L. Zhuang, J.T. Lu, J. Phys. Chem. C 111 (2007) 16416–16422.
[37] A. Katayama-Aramata, I. Toyoshima, J. Electroanal. Chem. 135 (1982) 111–119.
[38] N. Ikeo, Y. Iijima, N. Niimura, M. Sigematsu, T. Tazawa, S. Matsumoto, K. Kojima, Y. Nagasawa, Handbook of X-ray Photoelectron Spectroscopy, JEOL, 1991.
[39] G. Zhang, M. Liu, J. Mater. Sci. 34 (1999) 3213–3219.
[40] J.H. Kim, S.M. Choi, S.H. Nam, M.H. Seo, S.H. Choi, W.B. Kim, Appl. Catal. B: Environ. 82 (2008) 89–102.
[41] K. Ke, K. Waki, J. Electrochem. Soc. 154 (2007) A207–212.
[42] G. Samjeské, K. Komatsu, M. Osawa, J. Phys. Chem. C 113 (2009) 10222–10228.
[43] L. Jiang, L. Colmenares, Z. Jusys, G.Q. Sun, R.J. Behm, Electrochim. Acta 53 (2007) 377–389.